



Novel synthesis approaches for $\text{WO}_3\text{-TiO}_2\text{/MWCNT}$ composite photocatalysts- problematic issues of photoactivity enhancement factors



Enikő Bárdos^a, Gábor Kovács^{a,b,c}, Tamás Gyulavári^a, Krisztián Németh^a, Egon Kecsenovity^a, Péter Berki^a, Lucian Baia^{b,c}, Zsolt Pap^{b,c,d}, Klára Hernádi^{a,*}

^a Department of Applied and Environmental Chemistry University of Szeged, Rerrich Béla tér 1, HU-6720, Szeged, Hungary

^b Faculty of Physics, Babeş-Bolyai University, M. Kogălniceanu 1, RO-400084 Cluj-Napoca, Romania

^c Institute for Interdisciplinary Research on Bio-Nano-Sciences, Babeş-Bolyai University, Treboniu Laurian 42, RO-400271 Cluj-Napoca, Romania

^d Institute of Environmental Science and Technology, University of Szeged, Tisza Lajos krt. 103, HU-6720 Szeged, Hungary

ARTICLE INFO

Article history:

Received 30 September 2016

Received in revised form 25 February 2017

Accepted 15 March 2017

Available online 22 March 2017

Keywords:

WO_3 nanocrystallites

$\text{WO}_3\text{-TiO}_2$ nanocomposites

Photocatalytic activity

Carbon nanotubes

Photocatalysis

ABSTRACT

The “build-up” methodology, the importance of the order of the semiconductor layers in $\text{WO}_3\text{-TiO}_2\text{/MWCNT}$ composite materials was studied in terms of the applied synthesis pathway, morpho-structural parameters (mean crystallite size, crystal phase composition, morphology) and photocatalytic efficiency (using oxalic acid as model pollutant). The appearance of TiWO_x phase in the composites contributed to the enhancement of the photocatalytic efficiencies, as different synthesis approaches led to different crystal phase compositions. Although, it was proven that a beneficial phase's presence can be hindered if an excess of MWCNT or WO_3 was applied. As the ratio of the mentioned materials was reduced, active composites were obtained, but the previously noticed TiWO_x disappeared. Therefore, it was proven, that in the case of $\text{WO}_3\text{-TiO}_2\text{/MWCNT}$ nanocomposite system several photocatalytic activity enhancement factors can be introduced, but not simultaneously (the disappearance of TiWO_x at low MWCNT and WO_3 contents and the appearance of highly crystalline anatase).

© 2017 Elsevier B.V. All rights reserved.

1. Introduction

Catalysts are of great importance in the synthesis of petrochemicals, plastics, medical agents or fuel cell materials. Their applicability extends also for environmental applications, for example the reduction of emissions and degradation of various organic pollutants [1]. The catalytic activity and selectivity depend strongly on several parameters, such as crystal phase and stoichiometric composition, particle size and morphology, crystallinity grade of the catalyst or the shape of the catalyst nanocrystals [2,3]. Among the catalytic processes, photocatalysis is a very important alternative in the degradation of organic pollutants, and it is based on the irradiation of a semiconductor with photons of greater or equal energy than its band gap. Titanium dioxide (TiO_2) is a semiconductor metal oxide, which has many advantageous properties that makes it almost ideal for photocatalytic applications [4,5], it is photostable, biocompatible, non-toxic, relatively cheap and available in large quantity [6]. Under UV irradiation, it is an excellent

material for the degradation of various inorganic and organic compounds [7]. However, because of its large band gap energy, TiO_2 absorbs light only in the UV-A, near visible region. This is the main drawback of its wider application since only 4–5% of the solar emission spectrum falls in this range [8,9]. To overcome this problem there are many different approaches in the scientific literature. The most important methods to increase the photocatalytic activity contain catalyst modification by doping, metal decoration, surface sensitization, or by designing more efficient composites (e.g. mixed semiconductor oxides) [10], the latter possibility seems to be rather promising. Efficient charge separation can be obtained by the combination of two semiconductor particles that have different energy levels [11]. By properly tailoring the properties of the composite components, metal oxide heterojunctions can certainly be an interesting approach to modify the photocatalytic performances of individual oxides [12]. Every oxide component can display different chemical interaction with the contaminant to decompose. Surprisingly, in many cases oxide systems used for catalysis show many similarities with the ones investigated for sensing [13].

In the last few years, tungsten trioxide – titanium dioxide ($\text{WO}_3\text{/TiO}_2$) composite photocatalysts have drawn researchers' attention since they possess interesting and unique photocat-

* Corresponding author.

E-mail address: hernadi@chem.u-szeged.hu (K. Hernádi).

alytic features [14–16]. WO_3 shows a moderately small band gap energy, strong absorption within the visible spectrum, long-term performance and high chemical stability in a wide pH range of aqueous solutions under oxidative circumstances [17,18]. It is well-known in the literature that the connection between WO_3 and TiO_2 enables improved charge separation and visible light response [14–16,18–22]. Furthermore, WO_3 based composites possess a strong absorption in visible light, but their photocatalytic activities are very low.

Comparing band gaps of the two components (while relatively small – 2.4–2.8 eV – for WO_3 and high – 3.0–3.2 eV – for TiO_2) it is obvious that the transfer of electrons from bulk TiO_2 to WO_3 might further minimize the recombination losses.

Besides the above-mentioned composite formation of semiconductor oxides, the addition of carbon nanotubes (CNT) can be also a feasible method to elongate the lifetime of photogenerated e^-/h^+ pairs and prevent their recombination [23]. Because of their unique chemical, physical and electronic properties, CNTs are widely investigated [24,25] in order to promote applications in the field of composite materials and photocatalysts [23]. Since CNTs can act as an electron reservoir to store temporarily and transfer the photogenerated electrons from TiO_2 [25], with adding CNTs to the oxide, the photocatalytic activity of TiO_2 can be further improved [26–28] and possibly confer visible light activity [29]. The combination of the beneficial properties of WO_3 with the advantages of multiwalled carbon nanotubes (MWCNTs) can also result in a synergic effect to create materials with different properties for targeted applications. Thus, researchers have studied WO_3/MWCNT composites in previous works in order to investigate their gas sensing [30,31] and electrochromic performances [32]. Different impregnation methods were also presented to prepare WO_3/MWCNT composites: either a simple one-step fabrication method or combined with precipitation based synthesis techniques [33]. According to our knowledge, just a few publications can be found regarding the photocatalytic properties of ternary composites containing titanium and tungsten oxides with MWCNT. Literature data are rather inconsistent concerning the build-up methodology (synthesis approaches and oxide layer composition) of the above-discussed nanocomposites.

More synthesis approaches were already developed in order to investigate the available possibilities to obtain different contact order of the composite components. Two potential methods were identified: modified/slow hydrolysis (MSH) by Réti et al. [26], and impregnation (I) method which was investigated by Vass et al. [33]. These two approaches (combined a MSH) provided reliable results concerning the uniform coverage of MWCNTs with different semiconductor oxides (In_2O_3 , SnO_2 , Al_2O_3 , ZnO , $\text{SnO}_2\text{-In}_2\text{O}_3$). The advantages and drawbacks of these synthesis methods are summarized in Fig. 1.

In this paper, our interest is to clarify the effect of the heat treatment on the crystallinity and morphology of composite materials that were obtained by the methods listed above, while varying

the order of the different semiconductor layers and attempting to deposit simultaneously the two oxides (simultaneous slow hydrolysis and impregnation – denoted as SS method).

2. Materials and methods

2.1. Chemicals

All chemicals used were of analytical grade. The MWCNTs from Nanothinx (NTX1 type) titanium isopropoxide $\text{Ti}(\text{iPrO})_4$ and tungsten(VI) hexachloride (WCl_6) from Sigma-Aldrich, P25 from Evonik Aeroxide (Germany) were used without further purification for the preparation of the composite materials (secondary composites, for details please consult Sections 2.2 and 2.3)

2.2. Characterization methods

For measuring the DRS (Diffuse Reflectance Spectroscopy) spectra of the samples, a JASCO-V650 spectrophotometer with an integration sphere (ILV-724) was used ($\lambda = 250$ –800 nm).

The oxide layer thickness and coverage ratio of the oxides on the MWCNT were verified with FEI Technai G2 X-TWIN TEM (200 kV). The samples were prepared as follows: a small amount of the examined composite was sonicated in 1.25 cm^3 of ethanol. A few drops from this suspension were deposited and dried onto the surface of the grid (CF 200 Cu TEM grid).

The SEM micrographs were recorded on a Hitachi S-4700 Type II FE-SEM scanning electron microscope equipped with a cold field emission source operating in the range of 5–15 kV. The samples were mounted on a conductive carbon tape.

Powder XRD analysis was carried out on a Rigaku Mini-flex-II Diffractometer (angle-range: $2\theta = 20$ –80°, $\lambda = 0.15418 \text{ nm}$) using characteristic X-ray (CuK_{α}) radiation.

The Raman spectroscopy measurements were carried out on a Thermo Scientific DXR Raman microscope with a 532 nm laser (5 mW).

A photoreactor system with 2 LighTech 40 W fluorescent lamps ($\lambda_{\text{max}} \approx 365 \text{ nm}$, irradiation distance = 5 cm, irradiation time = 2 h) was used to measure the photocatalytic activities. The nanocomposites were grinded together with P25 (secondary composites) in order to differentiate their impact on the photocatalytic activity. The photocatalyst suspension containing oxalic-acid (initial concentration of oxalic-acid $c_{0,\text{oxalic-acid}} = 0.5 \text{ mM}$; $c_{\text{suspension}} = 20 \text{ mg}/20 \text{ cm}^3 = 1.0 \text{ g L}^{-1}$; total volume of the suspension $V_{\text{suspension}} = 20 \text{ cm}^3$) was continuously stirred during the experiments. The concentration decrease of the oxalic acid was followed using a Merck-Hitachi L-4250 system with Merck-Hitachi L-7100 pump. The eluent was H_2SO_4 (concentration of $\text{H}_2\text{SO}_4 = 19.3 \text{ mM}$), the applied flow rate was $0.8 \text{ cm}^3 \text{ min}^{-1}$ and the detection wavelength was 205 nm.

2.3. Preparation of nanocomposites

The $\text{TiO}_2\text{-WO}_3/\text{MWCNT}$ composites were prepared by slow hydrolysis and impregnation (SHI), a modified slow hydrolysis and impregnation, (MSHI) and a simultaneous synthesis (SS) method. The nomenclature of the composites contains the used method abbreviation (listed above) – first oxide – calcination temperature – second oxide – calcination temperature weight ratio of the components (just for those samples in which the ratio of the components was changed). If no heat treatment was applied for the specific oxide, the calcination temperature is denoted with 0. Examples: MSHI- TiO_2 -400-WO₃-450, MSHI- TiO_2 -0-WO₃-450. In the case of SS series the joint heat treatment temperature is included in the nomenclature – e.g. SS- TiO_2 -WO₃-700.

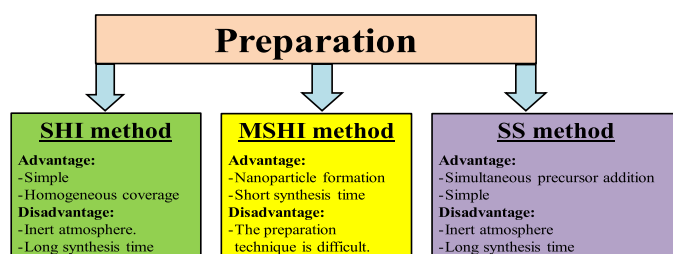


Fig. 1. The different preparation method advantages and disadvantages (slow hydrolysis and impregnation (SHI), a modified slow hydrolysis and impregnation, (MSHI) and a simultaneous synthesis (SS)).

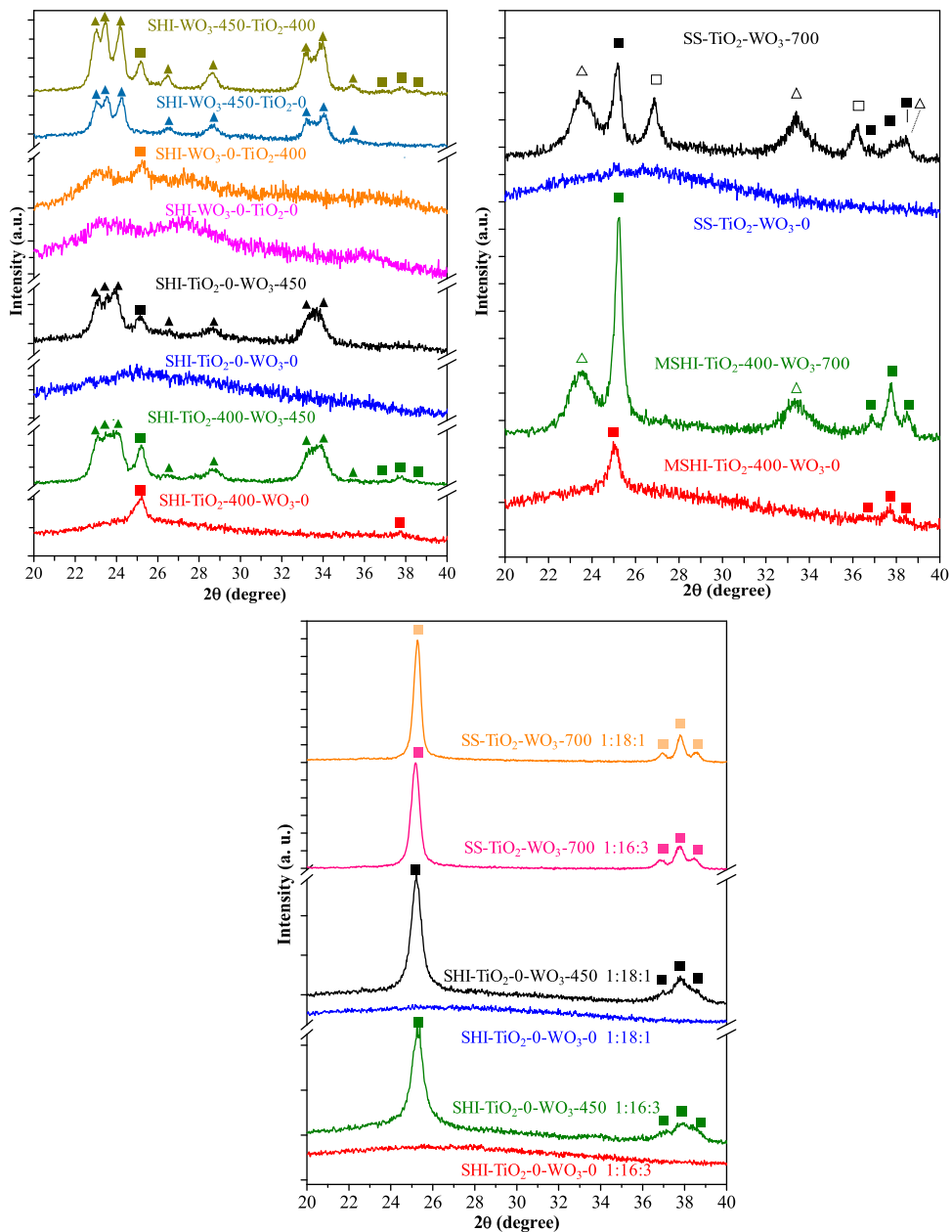


Fig. 2. The XRD patterns of the obtained composite materials (Δ – TiWO_x , \blacktriangle – monoclinic WO_3 , \blacksquare – Anatase TiO_2 , \square – Rutile TiO_2).

The addition of carbon nanotubes was decided as in the photocatalytic degradation process is presumably responsible for enhanced charge separation, as carbon nanotubes are efficient electron conducting materials, which can separate the electrons from the semiconductor, minimizing the chance of recombination. The composites made by SHI were prepared using an alkoxide precursor, titanium isopropoxide $\text{Ti}(\text{iPrO})_4$ and ethanol as solvent. The weight ratio of the reactants was 1:10:15 (MWCNT/TiO₂/WO₃). The dispersion of 100 mg MWCNTs and 150 cm³ ethanol was stirred vigorously under inert atmosphere (Ar) while the precursor (3.71 cm³) was added followed by a homogenization period of 1 h. The samples were kept at room temperature for a week until the solvent evaporated completely. The samples were separated into two parts: the first part was annealed at 400 °C for 3 h in air and grinded into fine powder in an agate mortar. The second part was not heat treated. For the impregnation method, TiO₂/MWCNT was applied as the raw material (both in annealed and not annealed forms) and WCl₆ as the precursor. Initially, 160 mg TiO₂/MWCNT

was added in 200 cm³ acetone and a suspension was prepared via sonication for 45 min. During this time, the calculated amount of precursor (257 mg) was dissolved in another portion of acetone (20 cm³). Finally, the solution of the precursor was added dropwise into the TiO₂/MWCNT-suspension and then the mixture was heated to 55–60 °C to evaporate the solvent on a heated magnetic stirrer. When the solvent was completely removed, a black powder was obtained. This powder was dried further at 90 °C for 24 h. The samples were annealed at 450 °C for 3 h in air. Composites were also prepared when the deposition order of the oxides was reversed.

The other TiO₂-WO₃/MWCNT composites were prepared by MSHI method. The weight ratio for the preparation was 1:10:15. 2.65 cm³ $\text{Ti}(\text{EtO})_4$ was added into 14.74 cm³ ethanol and homogenized using ultrasonication for 15 min to form the precursor solution. The dispersion of MWCNTs was stirred vigorously while the precursor solution was added dropwise. The molar ratios were n(TiO₂): n(H₂O): n(ethanol) = 1:3:30. After the addition of the pre-

cursor solution, the beaker was covered with plastic paraffin film and was stirred for an additional 1 h. After stirring, the samples were kept at 80 °C until all the solvent evaporated. Samples were annealed at 400 °C for 4 h in air and grinded into fine powder in an agate mortar. The impregnation process was the same like in the case of SHI method, but the samples were annealed at 700 °C for 3 h in inert atmosphere (Ar).

The composites were prepared also by the SS method: 100 mg MWCNT was added into 150 cm³ acetone homogenized by ultrasonication for 45 min. The dispersion of MWCNTs was stirred vigorously under inert atmosphere (Ar) while the Ti(iPrO)₄ precursor (3.71 cm³) was added. WCl₆ precursor (257 mg) was dissolved in another portion of acetone (20 cm³) and was added dropwise to the MWCNT dispersion. Then, the suspension was left to be stirred for 1 h. After stirring, the samples were kept at 23 °C for a week until all the solvent evaporated. Samples were annealed at 700 °C for 3 h in inert atmosphere.

For the photodegradation of oxalic acid, the previously described MWCNT-based composites and Evonik Aeroxide P25 were used for the preparation of the photocatalyst (secondary composites). In each case, a specific ratio was established between the composite components, 30% MWCNT-based composite and 70% TiO₂ (Evonik Aeroxide P25). The nanocomposites were prepared via mechanical mixing in an agate mortar for 3 × 5 min.

3. Results and discussion

3.1. Crystalline structure of nanocomposites

The XRD analysis of the obtained composite materials started with the samples SHI-TiO₂-400-WO₃-0 and SHI-TiO₂-400-WO₃-450. Both of them were obtained starting from heat treated TiO₂/MWCNT, which can be observed by the presence of the main anatase (JCPDS 21-1272) peak at 25 (2θ). In the case of SHI-TiO₂-400-WO₃-0, besides the anatase peak, only a baseline distorting was observed, behavior that indicates that WO₃ is clearly present as amorphous phase. When a supplementary heat treatment was applied at 450 °C the signals of monoclinic WO₃ emerged (JCPDS 43-1035, the mean crystallite size was of 20.2 nm). By applying this supplementary heat treatment, a slight increase of the mean crystallites size of anatase TiO₂, from 25 nm to 27 nm, was observed (Fig. 2).

The above-mentioned observations changed drastically, when the obtained TiO₂/MWCNT was not calcinated. Therefore, after impregnation with WO₃ precursor no sign of any crystalline material was detected (the case of sample SHI-TiO₂-0-WO₃-0). However, if a post calcination was applied, both signatures of anatase TiO₂ and monoclinic WO₃ appeared in the XRD pattern (SHI-TiO₂-0-WO₃-450), although a smaller amount of amorphous material remained as the pattern shows a slight increase in the main baseline. The mean crystallite size of TiO₂ and WO₃ was 29.9 nm and 74.0 nm, respectively.

Reversing the deposition order, another interesting aspect of these materials is revealed. If the WO₃/MWCNT initial composite was not calcined (composite SHI-WO₃-0-TiO₂-0) and the precursor of TiO₂ was deposited, a completely amorphous material was obtained (although there are signs of really small amounts of crystalline material). When a post heat treatment (composite SHI-WO₃-0-TiO₂-400) was applied, a small anatase signal appeared, while the rest of the material remained amorphous. No crystallite size calculation was possible in the case of these two samples.

To investigate the behavior of TiO₂, which was subsequently deposited, a prior heat-treatment to the WO₃/MWCNT composite was applied. After the impregnation process, the material contained only crystalline monoclinic WO₃, while no sign of any TiO₂

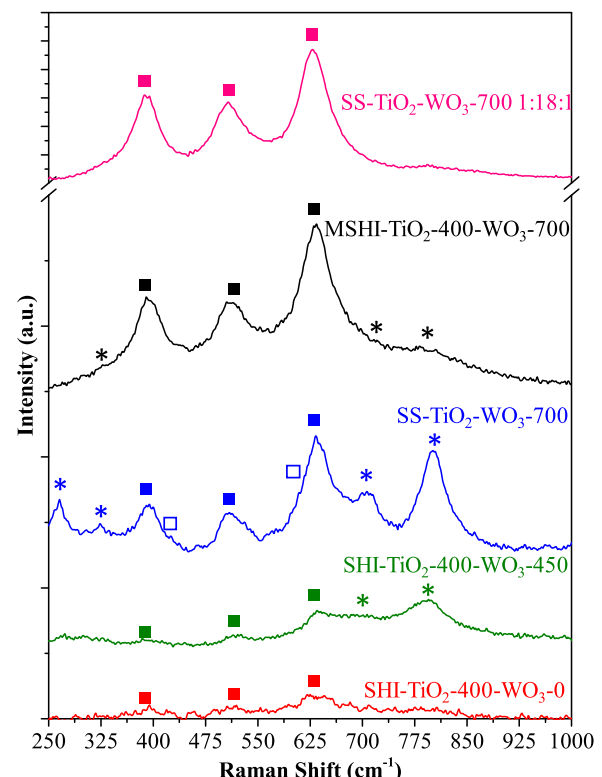


Fig. 3. The Raman spectra of the composite materials (* – WO₃ related bands, ■ – Anatase TiO₂, □ – Rutile TiO₂).

diffraction peaks was detected (sample SHI-WO₃-450-TiO₂-0). The mean crystal size of WO₃ was 28.4 nm. When the supplementary heat treatment was applied (sample SHI-WO₃-450-TiO₂-400), the anatase peak emerged, and the mean crystallite size of WO₃ increased slightly to 33.4 nm and the newly formed anatase crystals' size was 34.6 nm.

When TiO₂ was the first oxide deposited on the surface of MWCNTs, crystalline materials were obtained in three cases. When WO₃ was the first one, the final material was crystalline only in two cases. It seems like the pre-deposition of WO₃ inhibits the crystallization of the second oxide. This phenomenon was previously observed in literature [34,35]. Hence, the first strategy was further developed. As it was already detailed in the section focusing on the synthesis of these materials, the modified sol-gel and the simultaneous precursor hydrolysis strategies were applied.

The composite denoted as MSHI-TiO₂-400-WO₃-0 possess the same crystalline properties as the sample SHI-TiO₂-400-WO₃-0, namely they contain anatase phase with the same mean crystallite size. However, if a supplementary heat treatment was applied (this time at 700 °C, in order to further increase the crystallinity of the sample), new diffraction peaks appeared at 23.4 and 33.1 (2θ). These peaks reappeared in the case of the composite (SS-TiO₂-WO₃-700, while SS-TiO₂-WO₃-0 was completely amorphous), together with the already mentioned anatase reflections and the new ones attributed to rutile phase (the main diffraction peak at 27 (2θ), JCPDS 21-1276). Neither TiO₂ nor WO₃ crystal phases were identifiable by the peaks mentioned earlier. A possible explanation could be found in the work of Qureshi et al. [36], who shown the possible formation of TiWO_x, a rather surprising compound observed rarely in the last decade. TiWO_x appeared only in the 1:10:15 weight ratio samples. This means that a relatively high amount of WO₃ and MWCNT is needed to favor the formation of TiWO_x. Where the amount of the mentioned two components was lowered TiWO_x was not present at all. It should be also noted that

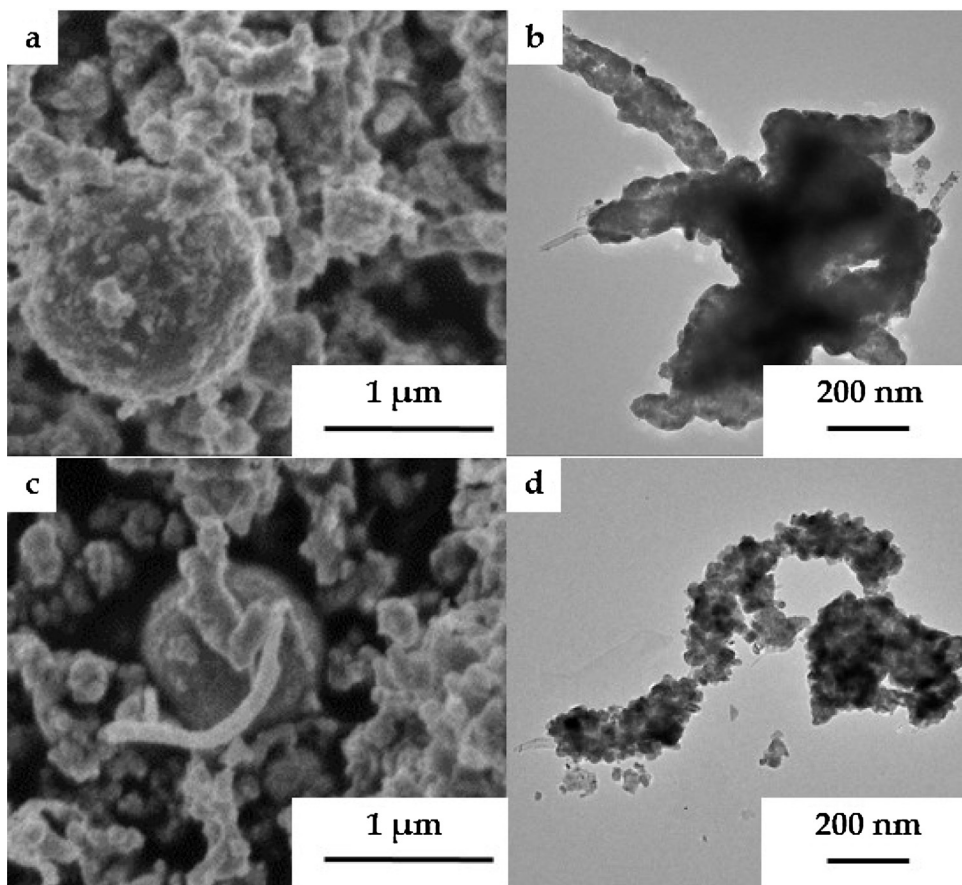


Fig. 4. Scanning (a,c) and transmission (b,d) EMs of TiO_2 /MWCNT-based composites (SHI- TiO_2 -0- WO_3 -450) and SHI- TiO_2 -400- WO_3 -450 (c,d)).

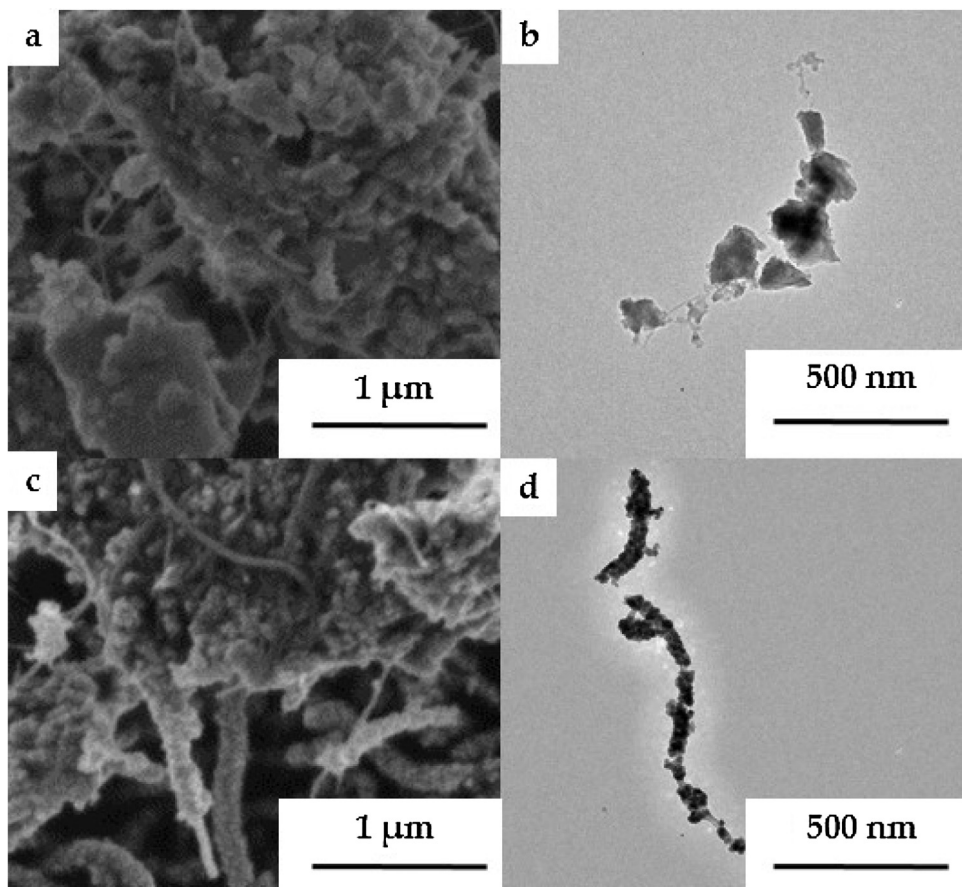


Fig. 5. Scanning (a,c) and transmission (b, d) EMs of WO_3 /MWCNT-based composites SHI- WO_3 -0- TiO_2 -400 (a,b) and SHI- WO_3 -450- TiO_2 -400 (c,d)).

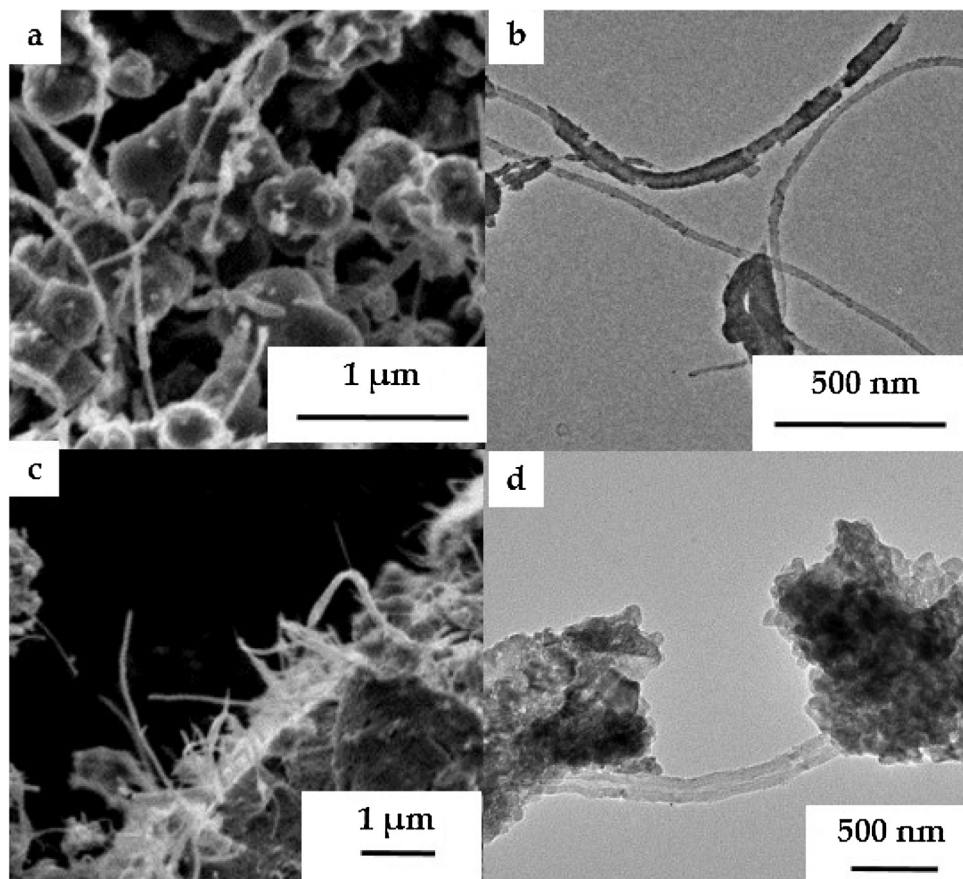


Fig. 6. Scanning (a,c) and transmission (b, d) EMs of composites MSHI-TiO₂-400-WO₃-700 (a, b) and SS-TiO₂-WO₃-700 (c,d).

the heat treatment was also crucial to obtain the above mentioned compound as it was obtained only when a calcination was applied at 700 °C.

The photocatalytic tests did not show any promising results as it will be detailed in Section 2.4, although two methods were involved (SS and SHI methods), which after further optimization could lead to photoactive composites. The strategy adopted was based on the fact that the CNT and the WO₃ 's relative content was rather high compared to TiO₂. Thus, the WO₃ and CNT contents were lowered (new component weight ratios 1:18:1, 1:16:3). When the XRD patterns were analyzed for these composites it was found that just anatase crystallized from the two oxides, while the non-heat treated samples were completely amorphous.

By comparing the mean crystallite size of these composites two important aspects can be pointed out. Thus, when the ratio of WO₃ decreased (relative to TiO₂) it was found that the crystallite size of the formed anatase slightly increased (from 16.3 to 17.4 nm – samples SHI-TiO₂-0-WO₃-450 1:16:3 vs. SHI-TiO₂-0-WO₃-450 1:18:1), in the case of sample series SHI and more intensively (from 22.4 nm to 47.5 nm – samples SS-TiO₂-WO₃-700 1:16:3 vs. SS-TiO₂-WO₃-700 1:18:1) when the SS method was applied. This observation emphasizes again that the presence of WO₃ inhibits the crystallization of TiO₂. Furthermore, at this ratio values, WO₃ does not appear at all in the XRD patterns indicating its potential dopant role.

It should be mentioned that in all the cases where WO₃ was not observable in the XRD, amorphous W(OH)_x is most probably the primary hydrolysis product, therefore no XRD peaks were expected and subsequently obtained.

The FT-Raman spectra reveal the presence of bands characteristic for TiO₂ anatase located around 144, 197 (these two were not included in the Figure), 394, 512, 638 and rutile phase at 445, 610 cm⁻¹ (both of them overlapped with anatase), respectively. The

D and G bands of the MWCNT did not suffer any modification, and therefore they were not included in Fig. 3.

The WO₃ crystalline structures (including tungstates) give rise to characteristic Raman bands around 710 and 800 cm⁻¹, while O—W—O bending modes are located at ≈260 cm⁻¹ and W=O stretching modes at 950–960 cm⁻¹ [34,35]. Most of the identifications made above coincide with the findings determined from the XRD results, therefore the observations made for samples SHI-TiO₂-400-WO₃-0, SHI-TiO₂-400-WO₃-450 and those with similar structures can be considered valid. However, it is interesting that the band associated with the presence of W=O units does not appear in the spectra of the investigated samples meaning that complete hydration (during hydrolysis) or non-stoichiometric species were formed. The band at 330 cm⁻¹, which corresponds to W-OH₂ stretching vibrations, suggested the previously enounced possibility, as these species appear when defective WO_x species are present [34,35]. This was also confirmed by the formation of TiWO_x identified by XRD.

Furthermore, if the ratio of the composite components is shifted in the favor of titania (while lowering the MWCNT and WO₃ content – sample SS-TiO₂-WO₃-700 1:18:1) the previously mentioned Raman bands, specific to WO₃, are missing, while the ones attributed to the presence of anatase TiO₂ intensified significantly. This information points out increased crystallinity, higher mean crystallite size and possible doping of anatase/amorphous WO₃.

3.2. Morphological investigations using scanning and transmission electron microscopy

Both SEM and TEM investigations revealed that carbon nanotubes were homogeneously covered by the binary oxide and the thickness of the layer was approximately 20–40 nm (Fig. 4a,b –

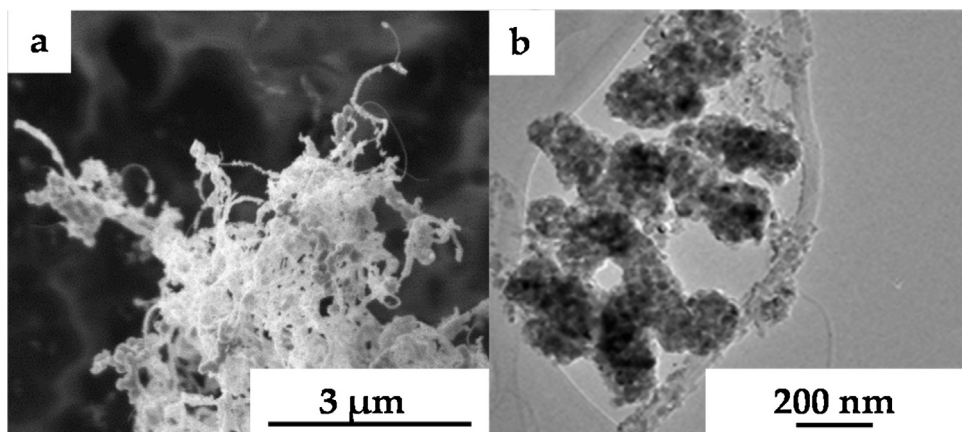


Fig. 7. Scanning (a) and transmission (b) EMs of changed weight ratio composites SS-TiO₂-WO₃-700 1:18:1.

sample SHI-TiO₂-0-WO₃-450). When TiO₂ was heat treated prior WO₃ deposition (Fig. 4c,d), the SEM and TEM micrographs showed that titanium dioxide and tungsten oxide evenly covered the surface of MWCNT, however, in many regions both oxides formed separate aggregates as well. From the micrographs it can be seen that the thickness of the layer was about 20–40 nm again and the size of detached oxide particles were in the range of 50–200 nm.

Changing the deposition order of the oxides on the MWCNT, it can be clearly seen from SEM and TEM micrographs that carbon nanotubes were not covered homogeneously with titanium dioxide and tungsten oxide (Fig. 5a,b), as mentioned previously, but larger aggregates of 100–500 nm size were formed and attached to the surface of MWCNT. However, when WO₃ received a heat treatment at 450 °C both SEM and TEM micrographs confirmed that carbon nanotubes were homogeneously and thickly covered by the binary oxide layer of approximately 100 nm (Fig. 5c,d).

In the case of the composites synthesized by modified slow hydrolysis and impregnation (MSHI), SEM and TEM measurements proved the coverage on the surface of carbon nanotubes (Fig. 6a,b). While the homogeneous region of the layer was composed of tungsten oxide, the titanium dioxide forms crystalline nanoparticles inside the coverage. The average thickness of the layer was of about 50 nm.

When the samples were prepared with simultaneous synthesis (SS) method Fig. 6(c,d) it cannot be seen homogeneous layer on the surface of MWCNT. SEM and TEM images show larger oxide particles of approximately 100 nm, randomly attached onto the carbon nanotubes. When the weight ratio was changed, the surface of carbon nanotube was covered homogeneously with titanium dioxide and tungsten trioxide. The average thickness of the layer was of 50–100 nm (Fig. 7a,b).

3.3. Optical properties of the individual WO₃ and composites

In order to evaluate the optical properties of the nanomaterials, diffuse reflectance measurements were performed on the composites with the best photocatalytic efficiencies. It can be seen in Fig. 8, that the materials absorb visible light in relatively high ratio (more than 80%). This behavior can be attributed to the higher MWCNT content in the composites (5%).

Due to the small light absorption edge, the band-gap values cannot be evaluated in the typical way, namely by the Kubelka-Munk equation, because the values obtained do not reflect the reality (values 4.0–5.0 eV). Therefore, the first order derivative of the DRS spectra (Fig. 9) was calculated in order to gain information about the electron transitions occurring during the irradiation of the nanomaterials, resulting realistic band-gap values.

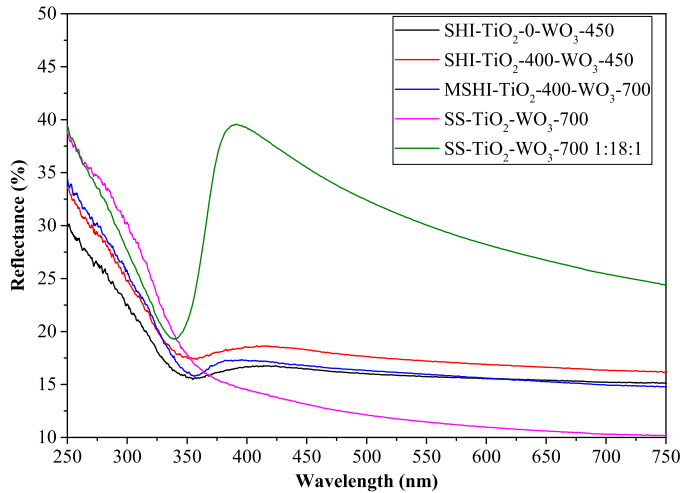


Fig. 8. The reflectance spectra of selected WO₃-TiO₂/MWCNT composites.

Analyzing the first order derivative of the reflectance data, mainly three electron transition bands can be seen, both responsible for the UV light absorption of the catalysts, at ≈362, 392 and ≈400 nm, respectively. These peaks, in terms of energy, are corresponding to the band-gap values of anatase, in the first case, to TiWO_x at 392 nm, and to monoclinic WO₃ for 400 nm. In addition to the qualitative presence of these transitions it is clearly visible that the differently synthesized composites have a change in the ratio of these peaks. Another aspect, which can be observed when WO₃ is deposited on the surface of the non-calcinated TiO₂/MWCNT samples, consists in that the peak of WO₃ cannot be observed on the first order derivative of the DRS spectra. This absence of the signal is most probably due to the presence of non-crystalline/amorphous WO₃, which “delays” the crystallization process of both semiconductors in the nanocomposites and may suggest a possible doping. When WO₃ was deposited on the thermally treated TiO₂-based material, the characteristic derivative peak of WO₃ appears around 400 nm, which means that the crystallization process is successful in this case, the semiconductor-oxide is “transformed” into its monoclinic form (results were proven also by XRD and Raman measurements, as discussed in Section 3.1).

As the ratio of the components was changed to 1:18:1 (sample SS-TiO₂-WO₃-700_1:18:1) anatase crystallized (a clear light absorption edge was visible in the DRS spectrum – Fig. 8), while no signs of WO₃ was detected in the XRD patterns and Raman spectra. As it can be seen in Fig. 9 the derivative spectrum does not show any additional bands, except the characteristic band of

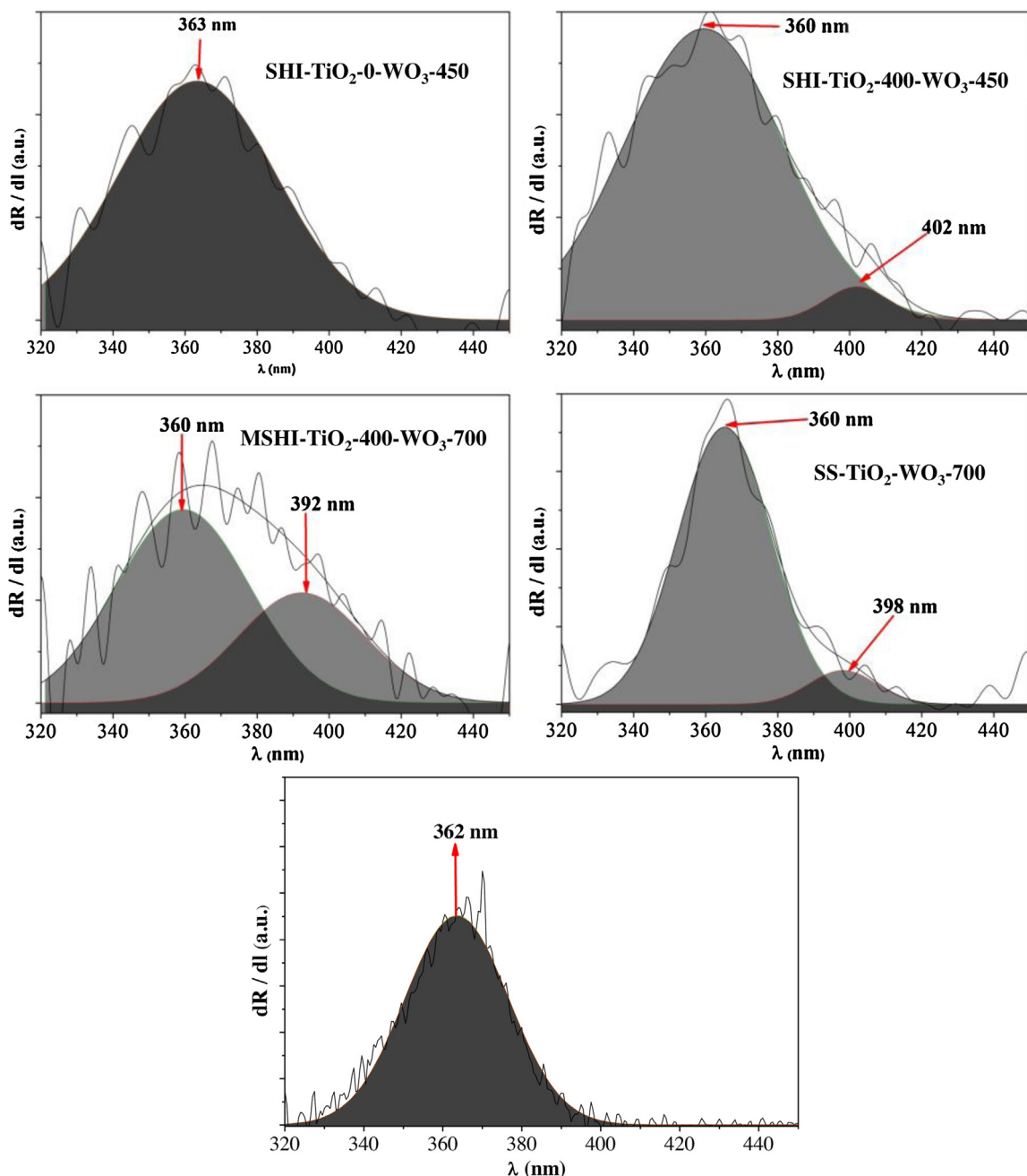


Fig. 9. First order derivative spectra of the $\text{WO}_3\text{-TiO}_2\text{/MWCNT}$ composites.

anatase at 365 nm. This explicitly points out that the WO_3 present in that sample must be amorphous [35].

3.4. Photocatalytic activity of $\text{WO}_3\text{-TiO}_2\text{/MWCNT-based nanocomposites}$

The initial composites were not active under UV irradiation. This result can be attributed to the relatively high amount of WO_3 present in the composite, and, as it is known from the literature, WO_3 has low photocatalytic activity under UV irradiation [37]. In order to gain further information about the photocatalytic potential of the composites a well-known commercial photocatalyst (P25) in a ratio of 70% P25 – 30% composite was prepared.

After two hours of photodegradation (Fig. 10) of oxalic acid, it can be concluded that the best performing composite was the

$\text{SHI-TiO}_2\text{-0-WO}_3\text{-450 + P25}$, with a degradation yield of 83.3% and the composite made by simultaneous synthesis (+P25) (75.1%). The $\text{SHI-WO}_3\text{-450-TiO}_2\text{-400}$ and $\text{SHI-WO}_3\text{-0-TiO}_2\text{-400}$ composites had a similar photocatalytic efficiency toward oxalic acid, both degrading less than 60% of the model contaminant (58.4 and 59.2%, respectively). The lowest efficiency was shown by the composite made by modified sol-gel synthesis, having a yield less than 40%. The commercial catalyst (P25) had the highest efficiency, decomposing 96.8% of the oxalic acid. This experiment pointed out clearly which of the involved synthesis methods could lead to the composite materials that may possess photocatalytic activity. Although the obtained composites deteriorated the activity of P25, the performed research pointed out which of the methods has potential to yield photoactive nanocomposites. The two most promising methods were chosen, $\text{SHI-TiO}_2\text{-0-WO}_3\text{-450}$ and $\text{SS - TiO}_2\text{ - WO}_3\text{-700}$.

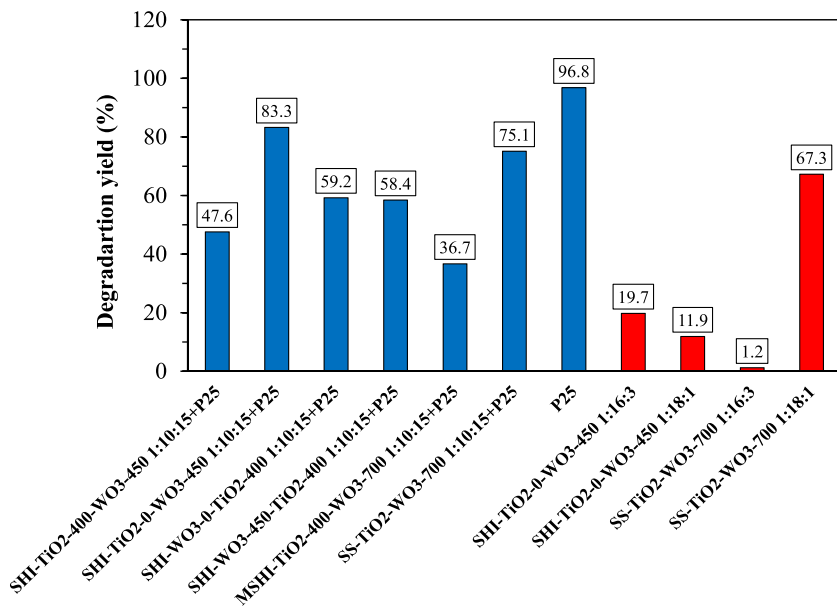


Fig. 10. Photocatalytic activities of various TiO₂-WO₃/MWCNT composites (composites obtained by the first synthesis approach and mixed with P25 – blue columns; composites obtained in the second optimization stage without P25 – red columns). (For interpretation of the references to colour in this figure legend, the reader is referred to the web version of this article.)

and their component contents further optimized: from 1:10:15 (MWCNT:TiO₂:WO₃) to 1:16:3 and 1:18:1.

The most efficient sample was the SS-TiO₂-WO₃-700 °C 1:18:1 weight ratio with a degradation yield of 67.3%. The other composites showed low photocatalytic performances, the SHI-TiO₂-0-WO₃-450 °C 1:16:3 degraded 19.7%, while the sample SHI-TiO₂-0-WO₃-450 °C 1:18:1 removed only 11.9%, and finally the sample TiO₂-WO₃-700 °C 1:16:3 was nearly inefficient (Fig. 10).

3.4.1. Searching for the origin of the photocatalytic activity of WO₃-TiO₂/MWCNT-based nanocomposites

Most of the samples showed very low photocatalytic activity, in which a crucial role was assigned to the composite components ratio. One of the chosen weight ratios of the composite components was 1:10:15 (MWCNT:TiO₂:WO₃), which showed a relatively high amount of WO₃ and MWCNT. As WO₃ has very low individual photocatalytic activity under UV irradiation [37], therefore, the activity deterioration could be ascribed with the highest possibility to the relatively high carbon content.

In order to enlighten the possible reasons for the obtained photocatalytic activity trend it was necessary to carry out additional investigations. One of the key structural features which might be responsible for the activity is the size of the specific surface area. We expected that a high value of the specific surface area results high photocatalytic activity, but the obtained results did not support this statement. The SHI-TiO₂-0-WO₃-450 (1:16:3) sample had a relatively high surface area (112.0 m² g⁻¹) however, the mentioned sample degraded only 19.7% of the oxalic acid compared to sample SS-TiO₂-WO₃-700 (1:18:1) which possessed 88.5 m² g⁻¹ surface area and showed a significantly higher degradation efficiency of 67.3%. Also sample SHI-WO₃-0-TiO₂-400 (1:10:15) should be pointed out, as it was the sample with the highest specific surface area, but no photocatalytic activity at all. Therefore, we concluded that, the photocatalytic activity was independent from the specific surface area in our case. The specific surface area values of all samples can be found in the supporting information (not all the values were introduced and discussed in detail as most of them showed low photocatalytic activity).

The four key samples were examined with XPS in order to investigate the source of the photocatalytic activity, as it was evident that

the surface quality was the key feature in our case. The XPS spectra of the samples revealed the same species in each of the composites. The main difference was in their concentration.

The X-ray photoelectron spectra (Ti2p, O1s, W4f) of sample SS-TiO₂-WO₃-700 1:18:1 are presented in Fig. 11. In the Ti2p XPS spectrum Ti⁴⁺ and a very small amount of Ti³⁺ (0.96 at.-% – peaks at 457.3 eV and 463.4 eV) along with Ti⁴⁺ (90.04 at.-% – peaks at 459.1 eV and 464.8 eV) [38] was detected, while in the O1s spectrum, the usual components in usual ratio were identified: oxide oxygen from TiO₂ (530.3 eV – 74.82 at.-%), surface OH group oxygen (531.3 eV – 21.78 at.-%), and oxygen from H₂O (532.8 eV – 3.40 at.-%). Furthermore, in the O1s spectrum of the materials no low binding energy oxygen species (528.8 eV) appeared. Based on our recent publications [38,39] this interesting oxygen type could be attributed to the presence of oxygen defects, or to oxygen atoms which are neighbouring to reduced Ti sites (i.e. Ti³⁺). In the samples SHI-TiO₂-0-WO₃-450 1:16:3, SHI-TiO₂-0-WO₃-450 1:18:1, SS-TiO₂-WO₃-700 1:16:3 the amount of Ti³⁺ increased gradually from 0.96 at.-% (SS-TiO₂-WO₃-700 1:18:1) to 3.21 at.-% (SS-TiO₂-WO₃-700 1:16:3), while the oxygen forms showed the same ratio. This means that the Ti³⁺ acted as recombination centers, consuming most probably the available holes, inhibiting the oxalic acid degradation by direct hole oxidation.

The W4f XPS spectrum of sample SS-TiO₂-WO₃-700 1:18:1 revealed two significant W species (W⁶⁺ and W⁴⁺ – 36.0/38.2 eV and 35.8/37.8 eV). W⁴⁺ presence conferred our materials a pale bluish color, as it was present in 21.2 at.% from the total amount of W. As WO₃ was not present in the XRD patterns of these samples, the most possible form of this oxide is amorphous with dangling, reduced W⁴⁺ sites, similar with the structure reported by Akurati et al. [40]. As the ratio of these species were unchanged in the other samples, emphasizing that in the case of these composites Ti³⁺ plays the activity defining role.

4. Conclusions

It is well known that due to its complexity photocatalysis can be influenced by many different parameters. Our investigation with a ternary composite system (WO₃-TiO₂/MWCNT) described here demonstrated this statement exemplarily. It was proved that not

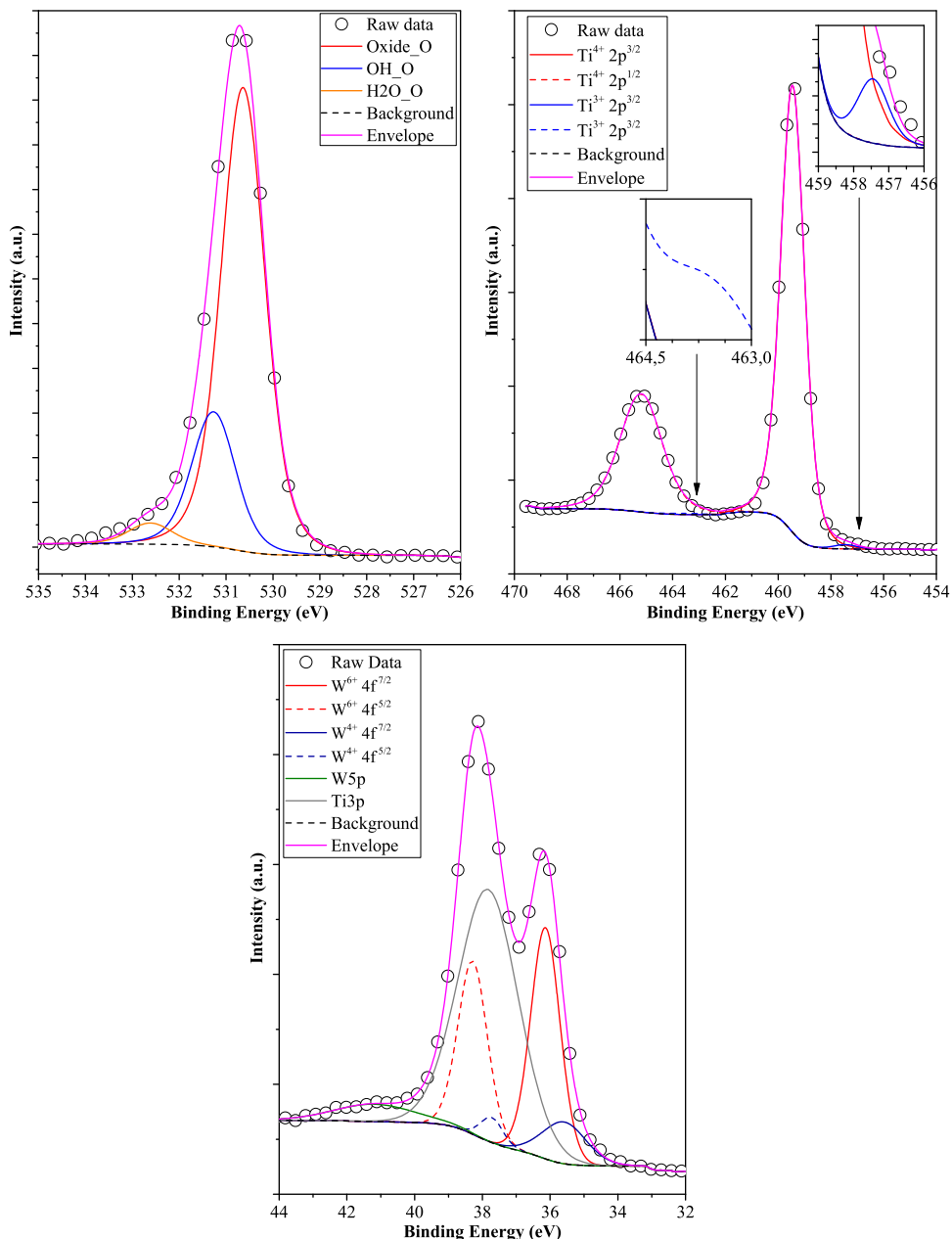


Fig. 11. XPS spectra (Ti2p, O1s and W4f) of sample SS-TiO₂-WO₃-700 1:18:1.

only the synthesis method but also the sequence of depositing the components (TiO₂ followed by WO₃), affect significantly the final properties of the nanocomposites. We have learnt that the properties of the oxide deposited in the first instance has a strong influence on the crystallinity of the second phase (e.g. different crystallite size of the individual oxide particles). At the same time, the higher degree of crystallinity does not necessarily coincides with the high photocatalytic activity (the example of SHI-TiO₂-0-WO₃-450). The appearance of TiWO_x crystal phase at higher temperature is also an interesting and somewhat unusual phenomenon and might be worth considering, since sample SS-TiO₂-WO₃-700 also showed promising photocatalytic activity. However, it cannot be stated that this new phase is exclusively responsible for the observed photocatalytic performances (see MSHI samples). This was proven, when the ratio of the composite components was changed, because in those samples TiWO_x disappeared and anatase crystallized with a high crystallite size, making it the main determining factor for the

photoactivity. Also, it is important that at low WO₃ and MWCNT content WO₃ does not appear at all suggesting a possible presence only as amorphous WO₃. Concerning the sequence of depositing the oxides it can be concluded that the existence of MWCNT-TiO₂-WO₃ junction is more advantageous. The photocatalyst showing the highest activity showed the lowest amount of Ti³⁺, emphasizing the role of recombination center of this species in these composites. Based on literature data [26] it cannot be excluded that the morphology of the composite components is also important.

Acknowledgments

This work was supported by a grant from Switzerland through Swiss Contribution (SH/7/2/20). G.K. wants to acknowledge the financial support of Hungarian Academy of Sciences, while Zs. P acknowledges the Premium Post-Doc project provided also by the Hungarian Academy of Sciences. The authors are also very grate-

ful to the financial support provided by the GINOP-2.3.2- 15-2016-00013 project.

Appendix A. Supplementary data

Supplementary data associated with this article can be found, in the online version, at <http://dx.doi.org/10.1016/j.cattod.2017.03.019>.

References

- [1] T.A. Saleh, V.K.J. Gupta, *Colloid Interface Sci.* 362 (2011) 337–344.
- [2] A.T. Bell, *Science* 299 (2003) 1688–1691.
- [3] K. Rajeshwar, A. Thomas, C.J. Janáky, *Phys. Chem. Lett.* 6 (2015) 139–147.
- [4] O. Carp, C.L. Huisman, A. Reller, *Prog. Solid State Chem.* 32 (2004) 33–177.
- [5] A. Fujishima, X. Zhang, C.R. Chim. 9 (2006) 750–760.
- [6] A. Mills, S.J. Le Hunte, *Photochem. Photobiol. A* 108 (1997) 1–35.
- [7] M.A. Fox, M.T. Dulay, *Chem. Rev.* 93 (1993) 341–357.
- [8] S. Banerjee, S.K. Mohapatra, P.P. Das, M. Misra, *Chem. Mater.* 20 (2008) 6784–6791.
- [9] Q. Li, L. Chen, G.J. Lu, *Phys. Chem. C* 111 (2007) 11494–11499.
- [10] N.A. Ramos-Delgado, M.A. Gracia-Pinilla, L. Maya-Treviño, L. Hinojosa-Reyes, J.L. Guzman-Mar, A.J. Hernández-Ramírez, *Hazard. Mater.* 263 (Pt. 1) (2013) 36–44.
- [11] S. Malato, P. Fernández-Ibáñez, M.I. Maldonado, J. Blanco, W. Gernjak, *Catal. Today* 147 (2009) 1–59.
- [12] K. Zakrzewska, *Thin Solid Films* 391 (2001) 229–238.
- [13] M. Epifani, E. Comini, R. Díaz, T. Andreu, A. Genç, J. Arbiol, P. Siciliano, G. Faglia, J.R. Morante, *Procedia Eng.* 87 (2014) 803–806.
- [14] S. Higashimoto, Y. Ushiroda, M. Azuma, *Top. Catal.* 47 (2008) 148–154.
- [15] C.W. Lai, S. Sreekantan, *Int. J. Hydrogen Energy* 38 (2013) 2156–2166.
- [16] A.K.L. Sajjad, S. Shamaila, B. Tian, F. Chen, J. Zhang, *J. Hazard. Mater.* 177 (2010) 781–791.
- [17] É. Karácsonyi, L. Baia, A. Dombi, V. Danciu, K. Mogyorósi, L.C. Pop, G. Kovács, V. Coșoveanu, A. Vulpoi, S. Simon, Zs Pap, *Catal. Today* 208 (2013) 19–27.
- [18] Y.-C. Nah, A. Ghicov, D. Kim, S. Berger, P. Schmuki, *J. Am. Chem. Soc.* 130 (2008) 16154–16155.
- [19] C. Das, I. Paramasivam, N. Liu, P. Schmuki, *Electrochim. Acta* 56 (2011) 10557–10561.
- [20] Y. Tae Kwon, K. Yong Song, W. Lee, G. Jin Choi, Y. Rag Do, *J. Catal.* 191 (2000) 192–199.
- [21] L. Sajjad, S. Shamaila, B. Tian, F. Chen, J. Zhang, *Appl. Catal. B* 91 (2009) 397–405.
- [22] V.M. Aroutiounian, V.M. Arakelyan, G.E. Shahnazaryan, *Sol. Energy* 78 (2005) 581–592.
- [23] K. Woan, G. Pyrgiotakis, W. Sigmund, *Adv. Mater.* 21 (2009) 2233–2239.
- [24] B. Lukic, J.W. Seo, E. Couteau, K. Lee, S. Gradecak, R. Berkecz, K. Hernádi, S. Delpeux, T. Cacciaguerra, F. Beguin, A. Fonseca, J.B. Nagy, G. Csányi, A. Kis, A.J. Kulik, L. Forró, *Appl. Phys. A* 80 (2005) 695–700.
- [25] J.W. Seo, E. Couteau, P. Umek, K. Hernádi, P. Marcoux, B. Lukic, Cs Mikó, M. Milas, M. Gaál, L. Forró, *New J. Phys.* 5 (2003), 120.1–120.22.
- [26] B. Réti, K. Mogyorósi, A. Dombi, K. Hernádi, *Appl. Catal. A* 469 (2014) 153–158.
- [27] C. Martínez, L. Canle, M. M.I. Fernández, J.A. Santaballa, J. Faria, *Appl. Catal. B* 102 (2011) 563–571.
- [28] N. Bouazza, M. Ouzzine, M.A. Lillo-Ródenas, D. Eder, A. Linares-Solano, *Appl. Catal. B* 92 (2009) 377–383.
- [29] L. Tian, L. Ye, K. Deng, L.J. Zan, *Solid State Chem.* 184 (2011) 1465–1471.
- [30] C. Balázsi, K. Sedláčková, E. Llobet, R. Ionescu, *Sens. Actuators B* 133 (2008) 151–155.
- [31] C. Bittencourt, A. Felten, E.H. Espinosa, R. Ionescu, E. Llobet, X. Correig, J.J. Pireaux, *Sens. Actuators B* 115 (2006) 33–41.
- [32] P.M. Kadam, N.L. Tarwal, S.S. Mali, H.P. Deshmukh, P.S. Patil, *Electrochim. Acta* 58 (2011) 556–561.
- [33] A. Vass, P. Berki, Z. Nemeth, B. Reti, K. Hernadi, *Phys. Status Solidi B* 250 (2013) 2554–2558.
- [34] G. Kovács, Zs Pap, C. Cotet, V. Coșoveanu, L. Baia, V. Danciu, *Materials* 8 (2015) 1059–1073.
- [35] G. Kovács, L. Baia, A. Vulpoi, T. Radu, É. Karácsonyi, A. Dombi, K. Hernádi, V. Danciu, S. Simon, Zs Pap, *Appl. Catal. B* 147 (2014) 508–517.
- [36] M. Qureshi, Prakash Gupta, *J. Chromatogr. A* 62 (1971) 439–448.
- [37] I. Székely, G. Kovács, L. Baia, V. Danciu, Zs Pap, *Materials* 9 (2016) 258.
- [38] Zs. Pap, É. Karácsonyi, Zs. Cegléd, A. Dombi, V. Danciu, I.C. Popescu, L. Baia, A. Oszkó, K. Mogyorósi, *Appl. Catal. B* 111 (2012) 595–604.
- [39] Zs. Pap, V. Danciu, Zs. Cegléd, Á. Kukovecz, A. Oszkó, A. Dombi, K. Mogyorósi, *Appl. Catal. B* 101 (2011) 461–470.
- [40] K.K. Akurati, A. Vital, J.-P. Dellermann, K. Michalow, T. Graule, D. Ferri, A. Baiker, *Appl. Catal. B* 79 (2008) 53–62.